30 August 2024
emils.kiselevskis@cern.ch
CERN, Geneva, Switzerland

# LINAC4 novel ion extraction system electrode material research

Emils Kiselevskis
Riga Technical University
Supervised by Dr. sc. Ing. Andris Ratkus

Keywords: Proton source, electrode, extraction system, conductivity, bonding, structural integrity

Abstract

The development and optimization of accelerator source charged particle extraction systems are central to improving ion source efficiency, electrode durability, and beam quality. These systems involve complex interactions between ionized particles and extraction electrodes, influenced by material properties like thermal conductivity and resistance to ion beam erosion. Materials like molybdenum, tungsten, and graphite are favored for their resilience in high-temperature, high-radiation environments. Challenges exist in bonding dissimilar materials under thermal stress. Techniques such as shrink-fit connections and additive manufacturing address these challenges by optimizing thermal expansion properties. Graphite and molybdenum carbide are ideal for additive manufacturing near a proton beam, with graphite requiring careful layer orientation. For materials not exposed to radiation, aluminum alloy AA7041 or pure copper are recommended. Advancements in additive manufacturing, including functionally graded materials, offer precise control over material properties, enhancing ion extraction electrode performance and lifespan.

## Contents

# 1 Introduction

CERN's linear accelerator Linac4 has been the main proton beam injector for the Large Hadron Collider since 2020, capable of accelerating the beam to 160 MeV. The Linac4 source system comprises a proton source and an extraction system. Negative hydrogen ions are created in ion source chamber when pulsed hydrogen gas is ionized with 100 kW power from a radio-frequency antenna. It creates mesh of hydrogen ions and extracted electrons, that are later separated from proton beam.

The design of the extraction system (see Figure 1) has evolved over time due to its significant impact on beam formation. Aim is to pull charged particles out of source chamber and create first formation of particle beam also by accelerating them. The latest IS04 source features three electrodes: plasma, puller, and ground electrode. Plasma electrode is often used as anode to attract oppositely charged particles towards aperture. Each electrode disk has a specific voltage and geometric shape. As the beam passes through the electrode system, it is shaped into a narrow formation with aim to reach lowest emittance. The free, co-extracted ions are directed into the electrode dump by a dipole magnet and a voltage of up to +1 kV, which helps eliminate secondary electron emission.

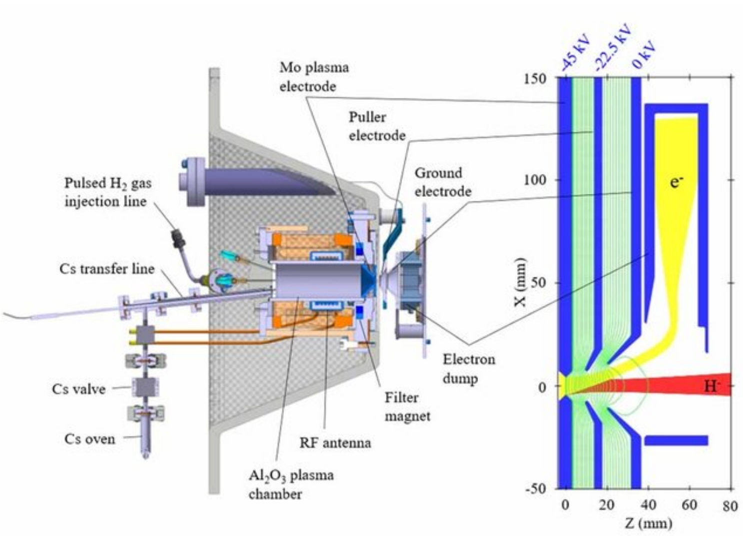


Figure 1: IS04 source 3D model (left) and extraction simulation model in IBSimu (right) [1].

At the end of the extraction system, the produced beam current is typically 35 mA. However, this current declines after passing through the RFQ (Radio-Frequency Quadrupole). Higher beam intensity does not increase intensity after the RFQ. Consequently, new extraction systems are being designed to more minimize the size of extraction system and extracted beam emittance, ensuring it does not exceed the acceptance limits of the RFQ [1].

As beam dynamics become more precise, relying on subtle changes in extraction electrode geometries, the mechanical characteristics of the electrodes also need to be considered. Factors such as thermal expansion, durability under high radiation loads, and the ability to withstand high voltages can significantly impact beam structure. The aim of this research is to enhance the overall performance and reliability of proton beam injectors by conducting a deeper investigation into the materials used in the beam extraction system and their constituent components using both conventional and additive manufacturing methods. This includes evaluating how these materials' mechanical properties influence the stability and efficiency of the beam extraction process.

The research process was based on the analysis of extraction systems used worldwide. Starting with solid materials and progressing to multiple material combinations, the study identified the proper functionality conditions of electrode structures. Combinations of materials were divided between conventional manufacturing techniques, such as shrink-fit technology, and the possible inclusion of additive manufacturing in the production of electrodes.

# 2 Investigation of extraction electrode material usage

This paragraph summarizes scientific researches or experience on charged particle extraction systems. Geometrical design impact has been investigated in numerous publications, therefore here will be summarized specifically – electrode materials. Research and commercially used accelerators mentioned in scientific journals, patents, and publications were taken into account. Therefore, due to information shortage, heavier ion source systems were also included as being with likewise characteristics. Each description includes visual material that helps to understand the application of the material for electrodes of various shapes.

## 2.1 Paul Scherrer Institute (Switzerland)

High intensity proton accelerator facility has reported usage of copper electrodes with small tungsten filaments near beam emittance part. The base material is aluminum (see Figure 2). This ion source tends to have low proton fraction, limited net proton current (11 mA) and high rate of damage at ion chamber bottom from back streaming electrons. Dimensions of electrodes are about 37mm in total length. Aperture of 4.5 mm in diameter. This system has experience breakdowns from copper evaporation in extraction system, that entered plasma chamber and condensed, creating "glassy" layer and stopping plasma ignition process [2].

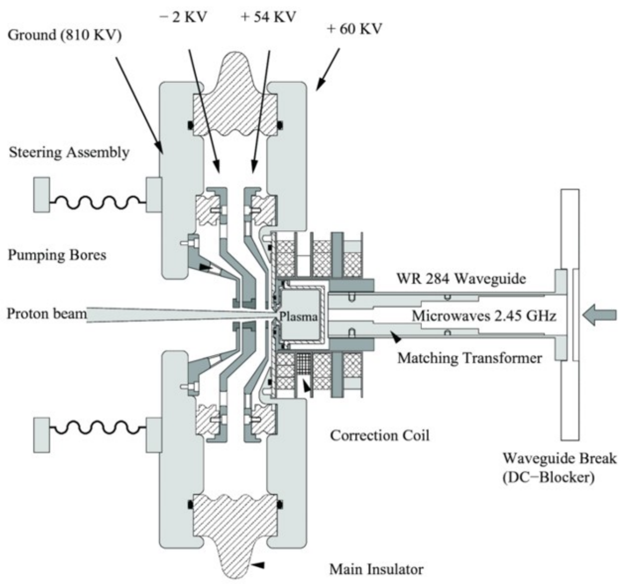


Figure 2: Schematic of the setup of the compact ECR proton source [2].

### 2.2 Stern-Gerlach-Zentrum (Germany)

The Frankfurt Neutron Source at the Stern-Gerlach-Zentrum used different material combination for proton ion source extraction electrodes. First puller electrode is almost completely made of tungsten and only very base of is made of copper (see Figure 3). Second electrode is partly tungsten and copper combination, but last two electrodes are only made of copper. Most parts of extraction system are made of special composite named elconite, that is copper and tungsten alloy. This indicates need of denser, radiation resistant electrode, as mentioned: "to reduce the surface sputtering and electron generation at the electrodes" [3].

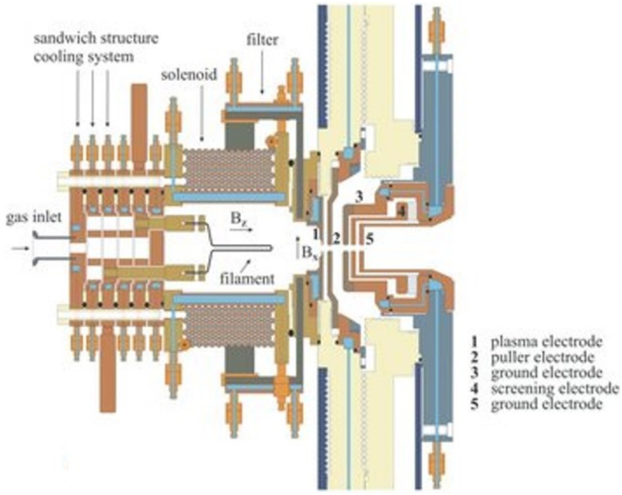


Figure 3: Schematic drawing fragment of the proton source [3].

### 2.3 Lanzhou university (China).

Institute of Modern Physics describes their first proton extraction system made in 1997, that was built of 2 electrode beam extraction system (see Figure 4) with electrode tips made out of TZM (molybdenum alloy "titanium-zirconium-molybdenum"). This system had accelerating and decelerating electrodes with gaps 6 mm and 3 mm respectively. Their updated extraction system was customized to fit CPHS (Compact Pulsed Hadron Source) proton source made with 3 electrode extraction, but there is limited mention about electrode material [4].

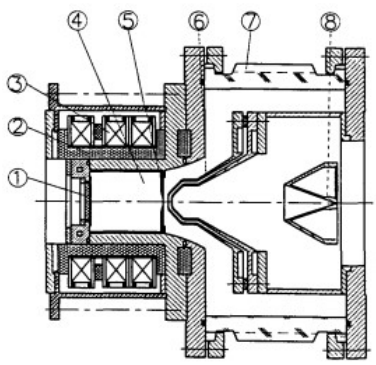


Figure 4: ECR ion source extraction system [4].

### 2.4 Egyptian Atomic Energy Authority (Egypt).

This paper primarily focuses on the design of an electrostatic lens system (see Figure 5). There were no mentions of electrode materials, as the main focus was on electrode placement and geometries. However, this paper highlights the tungsten usage as cathode material and the molybdenum usage as anode material. The ion source system has a built-in anode as part of the source system; therefore, it should not be equated with the plasma electrode (even though it has a pulling potential, it is not an independent electrode) [5]. Anode material molybdenum here is worth mentioning as it is located in a high-temperature, high-voltage, and high-radiation environment, that is similar to electrode environment.

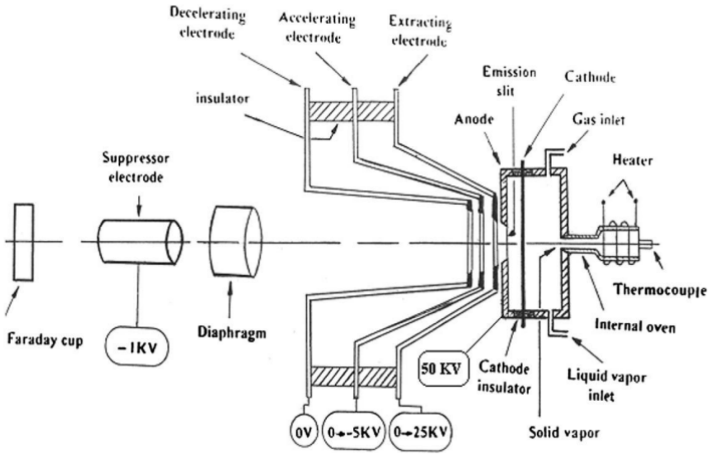


Figure 5: Schematic of the Freeman type ion source [5].

### 2.5 Nanjing University (China).

Nanjing Proton Source (NPS) proposed by Nanjing University has published triode extraction system (see Figure 6) with two conical shaped electrodes and separated flat plasma electrode. This system also uses molybdenum anode that can withstand large quantity of plasma induced heat power [6].

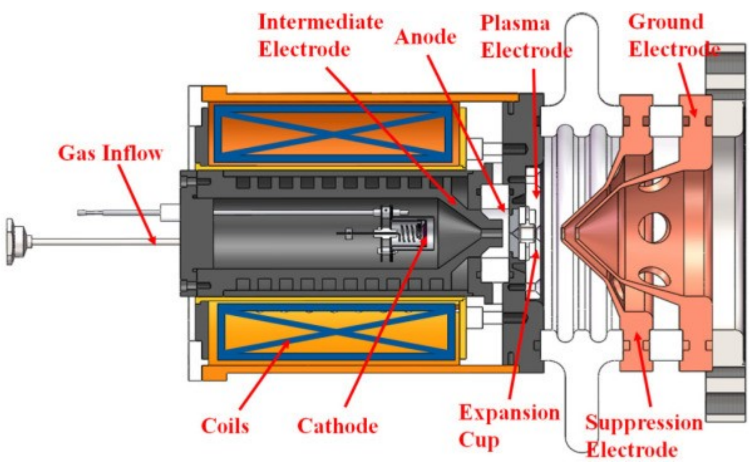


Figure 6: Structural drawing of the NPS duoplasmatron ion source [6].

## 2.6 CERN (Switzerland).

The Linac4 ion source, which operated around the year 2013 (see Figure 7), was the main ion source for the LHC injector complex. The Duoplasmatron source also included an anode component consisting of a molybdenum plate. The extraction electrodes are notable because they are made of titanium, which has rarely been mentioned before. However, this source had the disadvantage of being unable to maintain the 45 keV extraction energy, achieving only 35 keV. Electrons are dumped using a graphite cup, but a significant amount of damage to the graphite dump has been reported over a short period of time. Higher electron energy causes evaporation of the graphite material, leading to breakdown and dysfunctionality of the dump system [7].

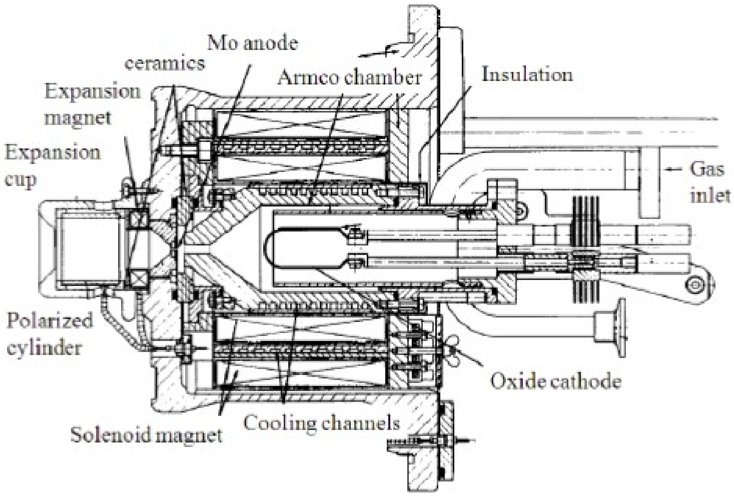


Figure 7: The CERN duoplasmatron proton source [7].

## 2.7 Axcelis Technologies (United States).

High current ion implanter patented in US in 2011 reports design of extraction electrode system consisting of 2 disk shaped electrodes and one extraction electrode to create proton beam (see Figure 8). The electrode system has 2 parts – first is single graphite plate with an opening or aperture and the second part is two matching graphite disk half assemblies with aperture in between disk halves. Edges of disks that form narrowing are replaceable if damage from accelerating ions occurs. This design can cut the cost by replacing only components with close contact to particle beam [8].

## 2.8 Budker Institute of Nuclear Physics (Russia).

This institute first began to use the negative hydrogen Penning ion source in the early 1970s (see Figure 9). This system uses hydrogen and cesium vapor feeding system into the discharge chamber. The beam is extracted from the plasma using high-voltage molybdenum electrodes [9]. It is important to note that the year mentioned reflects an older technology and does not represent the newest or most widely used ion extraction systems. But feeding system works on similar design as CERN Linac4 proton source.

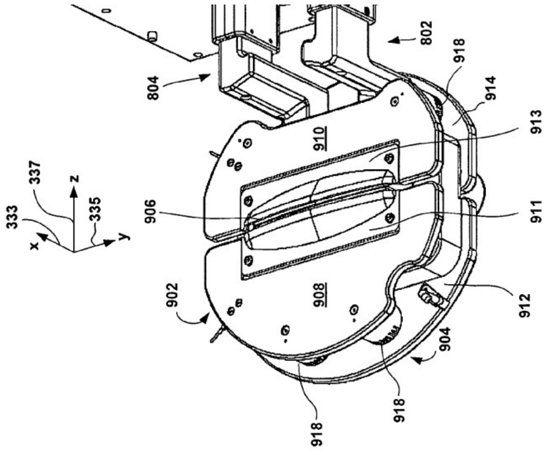

(a) Isometric projection of suppression disk half assembly.

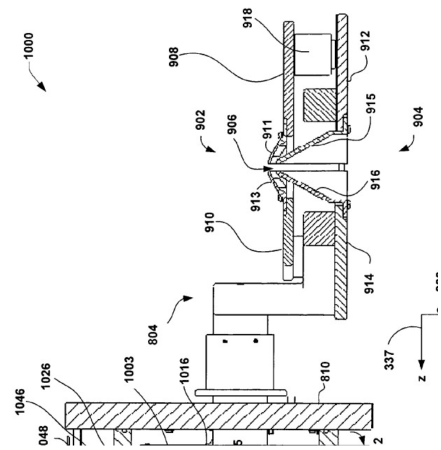

(b) Extraction electrode plate disk halves side view.

Figure 8: High current ion beam extraction system with replaceable components [8].

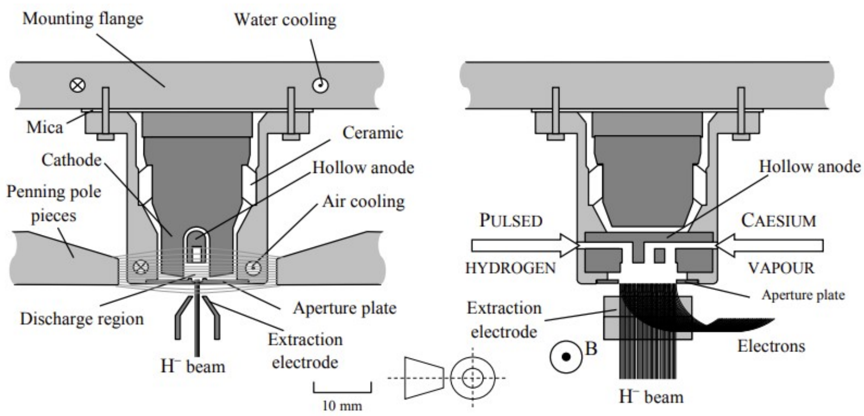


Figure 9: Sectional schematic of a Penning $H^-$ ion source [9].

## 2.9 University of Göttingen (Germany).

This source used the ultra-low energy ion implanter ADONIS, featuring a new ion source system for the ion implantation process (see Figure 10). This system has a different placement ion acceleration and control process, but charged particles are extracted from the ion source using an electrode similar to a plasma electrode. In this experiment, gas and later plasma were impacted through a different cathode-anode system for ion creation, with an acceleration potential of 30 kV. The report mentions two major materials used as accelerators: a tantalum cathode and a graphite anode for focusing and accelerating Argon plasma ions. Both conductive components are separated from each other by strong boron nitride (BN) insulators [10].

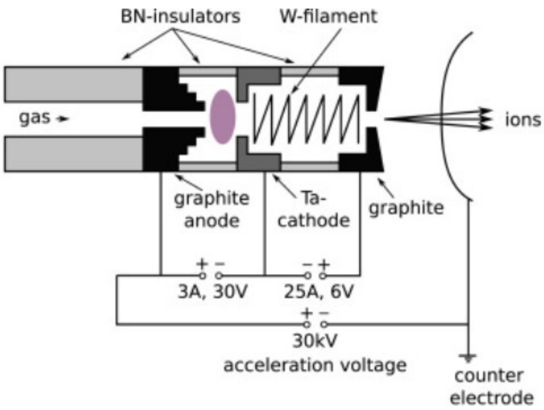


Figure 10: Schematic of the conventional hollow cathode hot filament source with the typical potentials [10].

### 2.10 Seoul National University (Korea).

Department of Nuclear Engineering reported research of high brightness ion beams with reducing aperture size to micrometer scale to see how ion beam current has changed. Their experimental setup (see Figure 11) consists of 3 electrode extraction system - plasma electrode, bias electrode, ground electrode, and insulators (ceramic disk 1mm thickness) between the electrodes. Ground electrode is made of aluminum, but all other are made of copper and they have water cooling channel. Accelerating voltage up to 4 kV is applied between plasma and ground electrodes. Results of experiment concluded that while smaller apertures typically increase brightness, they also significantly reduce beam current due to inadequate electric field penetration into the plasma source [11].

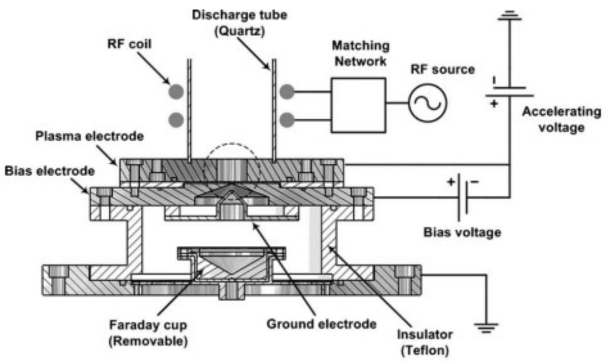


(a) Schematic diagram of the newly developed ion source including electrical connections.

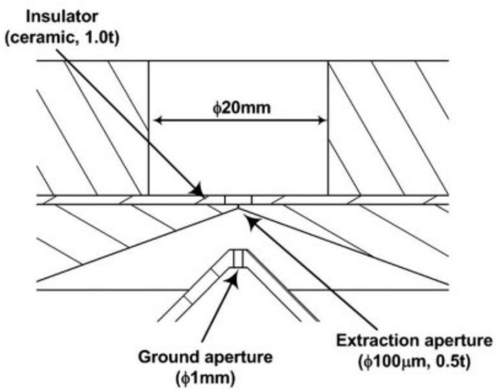


(b) Detailed drawing of extraction region enlarged from the dashed circle.

Figure 11: A schematic diagram of the ion source [11].

### 2.11 Doshisha University (Japan).

This source conducted deeper research on ion beam effects on electrode surface by investigating sputtering yields with a Monte Carlo simulation. Paper mentions use of graphite and molybdenum materials as most used ion beam extraction electrodes. Due to sputtered molybdenum and tungsten atoms from ion source system, atoms can reach extraction electrode surface and damage it, creating false geometries of apertures. Larger erosion pattern is detected on carbon graphite surface, but far less erosion on electrodes made of molybdenum. This result shows advantage of high material relative mass in respect to ion source elements – molybdenum has larger mass so it is less influenced by retained atoms [12].

### 2.12 Shin Etsu Chemical (Japan).

A patent describes an ion extraction electrode system where most ion beam processing parts use extraction electrodes made of graphite. However, these electrodes are prone to damage from the plasma beam, necessitating cleaning or replacement. To minimize electrode damage from heavy ions formed in the source, the inner surface of the ion source chamber, as well as the plasma contact side of the electrodes, is coated with a thin layer of silicon or carbon. This coating reduces the likelihood that the outermost ions, which might be heavy metal ions, will damage the electrodes by contaminating them. The solution also suggests using semiconductors such as germanium, GaP, InP, or GaAs. Long-term stability is achieved when the grounding and extraction electrodes are made from the same type of semiconductor substrate, ensuring compatibility. In the event of electrode damage, they will continue to produce the same type of ions, thereby maintaining purity and control [13]. Further beam contamination can be reduced with silicon and oxygen (range of 5 to 30 ppm) mixture that accepts heavy ions and they can be trapped within extraction or grounding electrodes. When using silicon as an electrode material, it is preferable, that electric resistance is within 0.001 to 10 $\Omega \cdot$ cm so pairing with similar electrodes can minimize electrical impact on the silicon substrates. Overall, this processing can lower maintenance cost, increase operational rates, improve productivity and increase yield [13].

### 2.13 Summary of material usage

Throughout these materials, molybdenum and graphite are considered as most used materials in beam extraction system electrodes. However, electrodes or anodes consisting of such metals are made solid and without connections or interactions to other conductive materials. Conductors such as copper and tungsten can be observed to be both involved forming one electrode manufacturing, most likely trough shrink-fit connection. Notable research was done in silicon usage as ion source inner coating. Extracted ions from such coating does less damage to electrodes while creating "outer layer" of beam than ions from heavy atoms ether from source or inner chamber walls. Further research could focus on replaceable electrode sections in the case of erosion or fracture.

Investigation can also be narrowed to TZM material investigation as it is one of the most popular molybdenum-based alloys, that's used with high temperatures. This material has high strength, low linear expansion coefficient, good electrical and thermal conductivity, strong corrosion resistance, that makes it suitable for long period usage. Better mechanical properties are reached with powder metallurgy method where high-purity molybdenum powder, $TiH_2$ powder, $ZrH_2$ powder, and graphite powder are mixed proportionally together [14].

Recent reports on the use of specific materials as extraction electrodes rarely specify whether the material is pure or an alloy. Therefore, further on when including aluminum, some outstanding alloys were selected based on the author's opinion. Aluminum alloys exhibit a range of properties, and for a deeper investigation, these alloyed materials should be examined further, particularly to characterize their impact on the solid substance. For most aluminum alloys containing Mg and Si, the thermal expansion coefficient increases more significantly in the temperature range from 50°C to 100°C. AlSi7Mg exhibits the lowest thermal expansion due to its high silicon saturation. Alloys with lower silicon concentrations, such as $AlMg_3Si1$, have higher expansion, especially at lower temperatures up to 100°C.

## 2.14 Summary of material properties

All materials mentioned in relation to ion source extraction manufacturing processes are compiled in Table 1.Based on recent advancements aiming to combine high-durability materials with aluminum, the table also includes some of the most notable alloys based on their properties. This table lists their specific physical and mechanical properties that are crucial for electrode functionality. A double line separates the materials based on their properties: those with high beam corrosion resistivity are listed at the top and can be used at point of contact with particle beam. Materials with higher conductivity, but lower durability are listed below and are more suitable further from high radiation environment.

The properties compared in Table 1 are selected based on the specific requirements for ion source electrodes. These properties include:

- **Thermal and Electrical conductivity**: These properties are crucial for ensuring the electrodes can operate effectively under high voltage conditions.
- **Thermal expansion, Melting point, and Radiation resistivity**: These characteristics are important for maintaining the material's fundamental geometry in the high-temperature particle beam environment. Radiation resistivity is not a scalar value, so the conclusion is drawn from the authors' overall research and opinion.
- **Yield stress**: Indicates the material's ability to resist plastic deformation, which is essential during the shrink-fit connection process.

Based on Table 1, it can be concluded that soft metals (listed in the bottom part) cannot be used in close contact with the radiation beam. A more cost-effective approach would be to use them as the base parts of electrodes to hold and create a transition to power source for materials that have high radiation resistance. Because of the operating temperature of the Linac4 extraction system, all the discussed materials are suitable for enduring the environment.

Evaluation of properties must be aligned with the requirements of the chosen manufacturing method. If additive manufacturing is selected, higher thermal and electrical conductivity is necessary. Thermal expansion should be low to prevent fractures on the product surface. Radiation resistivity should be high for electrode tip parts, while the base material does not require high resistivity. Yield stress should be maximized to ensure durable joints and products across all stress regions. The melting point is not predetermined - it depends on the production facility. For additive manufacturing, it is preferable for both materials to have similar melting points to ensure a smooth transition and complete melting of all structures. High radiation-resistant materials should have lower melting points, whereas lower resistance materials should have higher melting points, minimizing the difference between them.

From these conditions, it can be concluded that for additive manufacturing in close contact with a proton beam, graphite and molybdenum carbide (MoGr) are the most suitable materials. However, it is important to maintain the correct orientation of graphite layers due to its highly variable conductive and thermal expansion properties, which are a result of its allotropic nature. Additionally, it is preferable to use nuclear-grade graphite because of its higher thermal conductivity and yield stress. For materials not in close contact with the radiation beam, it is advisable to consider using aluminum alloy AA7041 or pure copper. These materials have the highest melting points among those close to radiation-resistant materials and are the best conductors. Pure aluminum could also be further investigated due to its good thermal conductivity, but it has the highest thermal expansion, which can lead to structural failures.

Table 1: Extraction system material properties

| Material | | Density [g/cm$^3$] | Thermal conductivity [W/(mK)] | Electrical conductivity [$\times 10^7$S/m] @20°C | Thermal expansion [$\times 10^{-6}$] @20-25°C | Melting point [°C] | Radiation Resistivity (H/M/L) | Yield stress [MPa] | References |
|---|---|---|---|---|---|---|---|---|---|
| Tungsten | W | 19.3 | 167.36 | 1.82 | 4.4 | 3'410 | High | 750 | [15] [16] [17] |
| Molybdenum | Mo | 10.2 | 138 | 2 | 4.8 | 2'622 | High | 345 | [18] [19] [20] [21] |
| Molybdenum TZM | Mo-0.5Ti-0.1Zr | 10.22 | 118 | 1.5 | 5.2 | 2'620 | High | 860 | [22] [23] [24] |
| Molybdenum Carbide – Graphite | MoGr | 2.5 | 85 [XY plane] 770 [Out-of-plane] | 0.03 [XY plane] 1.8 [Out-of-plane] | 12 [XY plane] 1.8 [Out-of-plane] | 2589 | High | 190 | [25] [26] |
| Titanium | Ti | 4.51 | 11.4 | 0.24 | 8.41 | 1660 | High | 240 | [27] [28] [29] |
| Graphite | C | 2.25 | 24 (C nuclear 200) | 0.005 [XY plane] 0.00003 [Out-of-plane] | 1.3 [XY plane] 25 [Out-of-plane] | 3'600 | Very high | 1.9 (nuclear 11700) | [30] [31] [32] [33] [34] [35] |
| Pure aluminum | Al | 2.69 | 238.66 | 3.54 | 23.8 | 660.2 | Low | 30 | [36] [37] |
| AA6061 | $AlMg_1SiCu$ | 2.7 | 167 | 2.46 | 23.6 | 617 | Low | 276 | [38] [39] [40] [41] |
| AA7041 | 97.64Al-0.84Mg-0.62Si-0.22Cu | 2.8 | *150-200** | *17** | 9.3 | *660** | *Medium** | *150** | [42] |
| EN AC-42000 | $AlSi_7Mg$ | 2.6 | 160 | 2.3 | 22 | 600 (mechanical limit 170) | Medium | 95 (-T64 exceeds 230 MPa) | [43] [44] |
| Al 4047 | $AlSi_{12}$ | 2.68 | 130-160 | 1.6-2.2 | 20.1 | 577 | Medium | 130 | [45] |
| Aluminum Silicon Alloy | Al-11.6Si-0.97Cu-0.96Mg-1Ni | *2.7** | *120** | *1.5** | *22** | *570** | *Medium** | *150** | |
| Pure copper | Cu | 8.9 | 401 | 5.7 | 16.8 | 1'083 | Medium | 33.3 | [46] [47] [48] [49] |

* No direct sources were found for other properties, indicating a lack of research on the mechanical properties. Information was gathered using artificial intelligence and the author's general knowledge.

# 3 Conventional multi-material electrode manufacturing

When using multiple materials in a composition, parts cannot be welded together due to the thin electrode walls and the risk of compromising structural integrity. The most commonly used method is the shrink-fit connection, which relies on the different thermal expansion coefficients of materials, expanding one part through heating or shrinking it by cooling in a cryogenic environment. Table 2 compiles the ability of recently discussed materials to be used in shrink-fit technology.

Physical bonding can also create specific environments that affect metals over time, although this has not been previously mentioned in the context of ion extraction systems. This paragraph examines such conditions and their potential impact on the functionality of bonded metals, particularly focusing on the bonding of commonly used materials like tungsten, copper, and aluminum.

## 3.1 Tungsten - copper connection

When connecting multiple different materials for creation of a part, it can be done ether by manual connection (tension) or using powder sintering. Each process strictly takes into account different thermal expansion coefficients, that can lead to geometrical deviations or structural failures. Especially, the difference of thermal expansion at 25°C for tungsten which is $4.5 \times 10^6$ and for copper which is $16.6 \times 10^6$. Such difference can induce joint failures when thermal stress is too high and not designed adequately. Ability of copper to conduct heat can be used in system also as a cooling structure [50].

## 3.2 Tungsten - aluminum connection

So far there are no direct source of information, that covers experience of aluminum and tungsten bonding. It is possible to consider use of aluminum-tungsten alloy, but there are also no valid source of information with possible results or functionality of W-Al alloy. Only one source states low cost of manufacturing and tensile strength of more than 300 MPa at room-temperature, that can improve tungsten endurance at relatively low ambient temperature [51].

Atomic interaction forces can be detected at the boundary between aluminum and tungsten materials. At a certain distance between these materials, a stronger chemisorption interaction occurs between the aluminum surface atoms and the tungsten surface, resulting in the transfer of aluminum atoms to the tungsten surface. This interaction is nonlinear and reaches its highest force gradient at distances of 4.5 to 7.9 Å. At this range, the force gradient is negative, meaning that increasing the distance initially increases the interaction force, which then decreases significantly when the distance is less than 4 Å. It is important to note that these interactions and experiments are conducted on clean aluminum and tungsten surfaces. The active oxidation process of the contact surfaces is inevitable; therefore, it must be minimized chemically or physically before the connection is made [52].

## 3.3 Overview of conventional material connections

As long as the two bonded materials have similar properties, overall functionality of system may be reduced on border of changing environments, but it will not be significantly impacted if both materials can conduct electricity. The quality of the connection is crucial - closer contact between the surfaces (with minimal air gaps) results in better conductivity. To improve the connection between two metals, either the lowest possible surface roughness or the use of soldering paste is recommended.

Based on Table 2 almost all material combinations are possible, as long as the induced shape change is sufficient to ensure a strong bond. The connection between tungsten and aluminum exhibits better material activity at the boundary, with aluminum being preferred when saturated with silicon. All aluminum alloys, as well as copper, are good thermal conductors, making them suitable for the shrink-fit method. However, graphite-saturated materials should not be used in shrink-fit connections due to the unreliability of expansion direction. As an allotropic material, graphite expands asymmetrically, and errors in manufacturing can lead to weak material connections.

Table 2: Materials Overview for Shrink-Fit Applications

| Material | | Shrink-fit | Evaluation | Reference |
|---|---|---|---|---|
| Tungsten | W | Yes | Usually not used pure material, because of poor machinability. Used as carbide or copper alloy. Then it is chilled in dry ice or nitrogen. Advised to use .005in/.007in interference per side. | [53] [54] |
| Molybdenum | Mo | Difficult | Molybdenum has low thermal expansion coefficient. It can only be used as cooled inserts and under large cooling temperatures. | [55] |
| Molybdenum TZM | Mo-0.5Ti-0.1Zr | Difficult | Less used in manufacturing due to highly expensive costs of substances. Can be stable in temperature above 1400°C, that makes hard to maintain heat for expansion. | [56] |
| Molybdenum Carbide Graphite | MoGr | *Difficult*[*] | *Graphite component ensures easier connection where friction is dominating. High work temperature ensures outstanding connection when cooling and shrinking material back to ambient temperature.*[*] | |
| Titanium | Ti | Yes | Alloys (Grade 23 / Grade 5) are more resistant, but harder for machinability than pure Ti. Cooled with liquid nitrogen (-160°C). | [57] |
| Graphite | C (crystalline form) | Yes | Used for cold fitting and shrink fitting. For shrink fit bearing system ISO tolerances are advised H7 for housing diameter and for bearing before D8, after E8...E9. Nominal interference advised 750 µm. | [58] [59] |
| Pure aluminum | Al | Yes | Does not get brittle at cryogenic temperatures and has high thermal expansion coefficient. When cooled in liquid nitrogen, aluminum gets highly flexible. Can also be used as housing material for other heated elements with high thermal expansion. If aluminum is heated, it exhibits shrinking rate from 0.4% to 0.7%, meaning shrink fitting will obviously not exceed lower margin. Lack of studies with each alloy means considering materials with higher thermal conductivity and yield stress. | [36] [37] |
| AA6061 | AlMg1SiCu | | | |
| AA7041 | 97.64Al-0.84Mg-0.62Si-0.22Cu | | | |
| EN AC-42000 | AlSi7Mg | | | |
| Al 4047 | AlSi12 | | | |
| Hypereutectic Aluminum-Silicon Alloy | Al 11.6Si 0.97Cu 0.96Mg 1Ni | | | |
| Pure copper | Cu | Yes | Good conductor, so heated during fitting. Copper shrinks at a rate of 0.5% to 1.5% after casting process, meaning shrink fitting will obviously not exceed lower margin. | [37] |

[*] No direct source was found for the previous use of such technology. Information was gathered using artificial intelligence and the author's overall understanding of each composite material.

## 4 Multi material additive manufacturing

Two material bonding can be achieved using additive manufacturing. Usually, this technology is used to compose 1 material 3-dimensional structure by melting metal powder and forming desired shapes. Therefore, functionally graded materials are used - heterogeneous structures with different micro-structure, where composition and properties can be achieved with multi-material composition and consists of at least 2 material combination. Bonding can be discrete (definable boundary) or graded (continuous boundary) (see Figure 12). Both bondings can be described in 2D form that forms two "layers" and 3D form that results in material transition in at least two dimensions. Best bonding is determined by similarity of both material atomic bonding and coefficient of thermal expansion. So far most used are Fe and Al alloys for 2D; Cu and steel for 3D. Deformation in interference zone can be minimized by determination of suitable geometries along the interfaces or optimization of the process parameters. Advanced software is preferable to simulate and optimize melt pool geometry and investigate heat input, thermal emission, phase transition and surface tension [60].

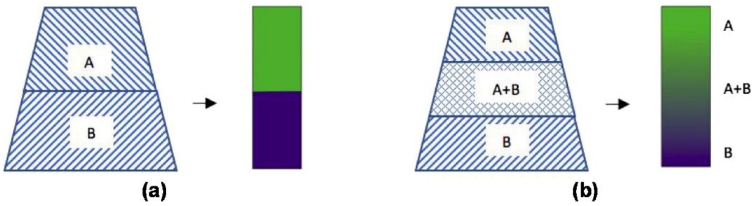


Figure 12: (a) Conventional multi-material additive manufacturing *vs.* (b) functionally graded MMAM (Multi-material additive manufacturing) [61].

For multi-material combination used are various blendings of polymer, metal, ceramic. Electrodes are metal saturated, therefor metal-metal feeding unit is required with most focus directed on compatibility of boundary. With direct energy deposition method (DED) high strength and high ductility products can be acquired. DED process known as laser metal deposition (LMD), where powder is added onto melt pull while being heated with moving laser, powder composition can be changed between layers. This technique has already been used with titanium and nickel alloys, steel and metal matrixes. This does not require special tooling, but performance limits depend on abilities of AM machining. Biggest challenge is mismatch between thermal conductivity, expansion and melting points of both materials [61].

For multi-material manufacturing, the powder bed fusion method (PBF) is also possible (see Figure 13), where a layer of metal powder is deposited onto a substrate using a powder feeding system. The powder is then rolled over the previous layer and sintered with a heat source, typically a laser or electron beam. When using multiple materials with dissimilar melting characteristics, it is critical to optimize the melting area by utilizing smaller particles for the higher melting point material. This increases energy absorption and helps to reduce the formation of cracks between the dissimilar materials. [61].

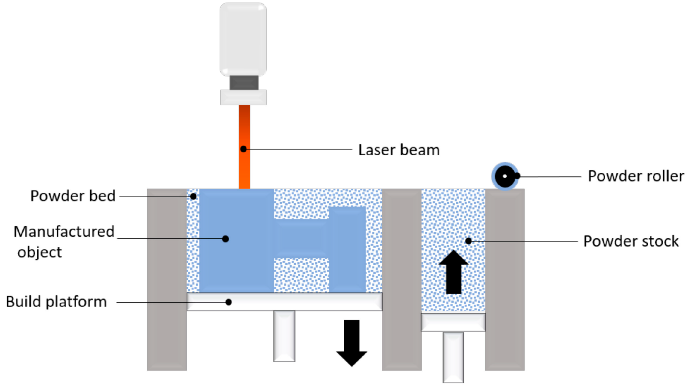


Figure 13: Schematic representation of PBF [62].

Usual DED build up direction is vertical without angle. In case of extraction electrode manufacturing, they are generally cylindrical in shape, with the upper part bent at a noticeable angle. When powder feeding system is co-axial (symmetrical from both sides) and equipped with 350W laser, then additional material buildup can be observed when angle is increased (see Figure 14). When research was done with Fe-Ni-Cr super alloy, this results in increased wall thickness for $\sim$ 45%. Minor changes in wall parameters observed till 20$^o$ angle. Wall structural failure (deformation) observed at 32.9$^o$. Angles till 30$^o$ are named as stable [63].

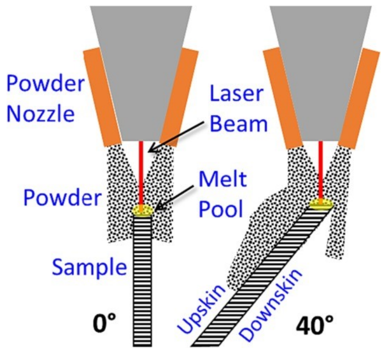


Figure 14: Example of powder impingement for vertical and angled sample [63].

Similar experiment with direct energy deposition with buildup in certain angle was done observing changes in Ti-6Al-4V structure. Here laser has power of 450W and forming of structure was narrow to observe structural integrity with minimal structural support at maximum overhang angle. 50.8mm long structures were successfully deposited between 0$^o$ and 60$^o$. As the laser turns off, the melt solidifies, starting from the bottom and sides, allowing overhang formation. Continuous wave (CW) lasers cannot form highly-overhanging structures because they prevent proper solidification, leading to large, unstable melts. Without the solidification of the melt's edges, the upward formation becomes impossible [64].

Multi material feeding systems can solid-state and powder state. Solid-state feeding system consists of one (see Figure 15) or two material wires (multi-wire feeder), that can increase or decrease feed rate independently, creating smooth transition. Powder-state feeding system can use powder disposing system, but its greatest challenge is powder agglomeration during feeding. Therefore, ultrasonic micro powder dispensing has been used with applying ultrasonic vibrations to powder to create it more fluidize and dispensed accurately. Such system expresses material consistency better, improved productivity, waste reduction, higher compatibility between materials and improved strength and surface finish [65].

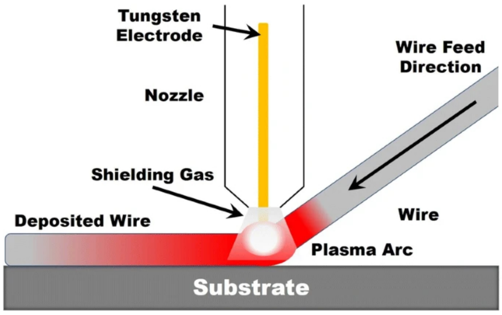


Figure 15: Schematic of pulsed plasma arc wire-fed DED additive manufacturing [66].

When high melting temperature and Yield stress materials are used (for example Niobium and Titanium), Nb powder melted partially, creating accumulation in transition zone, improving hardness. For this method it is suggested to use fine particles to avoid precipitations of non-melting particles [65].

From the perspectives of production cost and capabilities, we can conclude that the previously discussed methods - DED, WAAM (Wire arc additive manufacturing), and PBF, where laser melting of powder or wire is involved - might not be the most cost-effective or accurate methods (see Figure 16). DED tends to have poor surface quality, but this is a common drawback across most additive manufacturing methods. However, DED does produce products with some of the highest mechanical strength. The WAAM method can be less expensive while still offering good surface quality and accuracy. PBF, although is relatively slow and costly, but provides very good part accuracy [65].

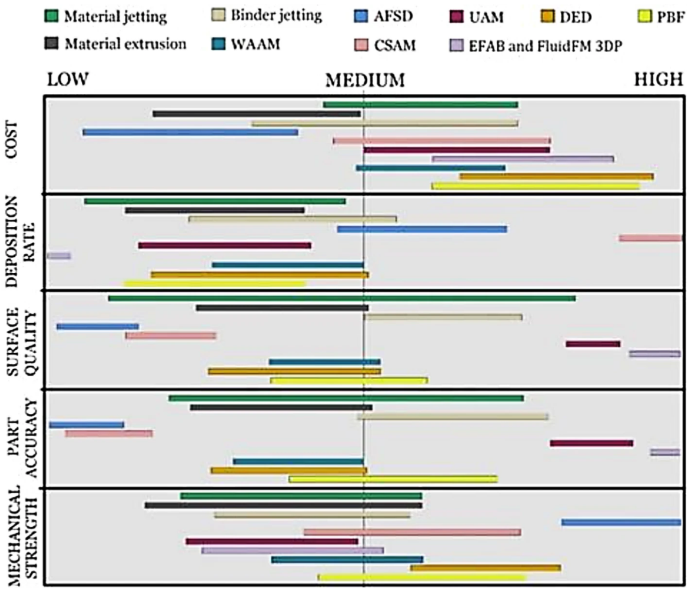


Figure 16: (AFSD - Additive friction stir deposition; UAM - Ultrasonic additive manufacturing; CSAM - Cold spray additive manufacturing; EFAB - Electrochemical fabrication) Comparison of AM Processes based on the cost, deposition rate, surface quality, part accuracy and mechanical strength [65].

Overall, these three methods are also suitable for multi-material manufacturing and share similar characteristics. PBF offers the highest surface quality, potentially reducing the cost of surface treatment. However, the most important parameter is part accuracy, where PBF delivers the best results.

Multi-material or single-material additive manufacturing has great potential for replacing conventional electrode manufacturing methods. Alloyed materials can be easily mixed just before the direct energy deposition method, and materials can be combined in their powder state. Despite this, the lack of studies on materials with significantly different melting points raises uncertainty about combining such materials while ensuring a durable connection. Despite the fact that the low proton source temperature can help maintain a lower thermal stress environment, optimization can be done on the length of the boundary, creating simpler and smoother transition zones. So far, copper and molybdenum alloys appear to be promising materials for further research, based on their closest melting points within the two different groups of electrode materials with high radiation resistance.

## 5 Conclusion

Of all the reviewed electrode materials in Table 1, graphite and molybdenum carbide are the most suitable for use near a proton beam due to their resistance to high temperatures, radiation contamination, and high-voltage conditions. For graphite, maintaining proper layer orientation is crucial because of its better electrical conductivity and lower thermal expansion properties at XY plane. Nuclear-grade graphite is preferred for its superior thermal conductivity and yield stress. For materials not in direct contact with the radiation beam, aluminum alloy AA7041 or pure copper are recommended due to their high melting points and excellent conductivity. Higher silicon saturation in aluminum alloys lowers thermal expansion, making them more suitable for various types of manufacturing.

Shrink-fit technology is applicable to almost any electrode material connections as long as both exhibit different thermal properties. Radiation-resistant materials often have significantly different thermal expansion properties compared to conductive base materials. If using graphite and molybdenum carbide, expansion mismatches can pose disadvantages when a shrink-fit connection is used, therefore, molybdenum products can be better manufactured using powder-based additive manufacturing methods. Graphite exhibits asymmetrical expansion so offsets in manufacturing process can lead to unsimilar material connections.

Additive manufacturing offers a versatile approach for fabricating electrode materials, especially when a homogeneous and continuous boundary is required. This method is particularly suitable for materials like aluminum alloy AA7041 or pure copper, which are not in direct contact with the radiation beam. These materials, known for their high melting points and excellent conductivity, are compatible with powder bed fusion technology, where laser-induced heat treatment can enhance material strength. Powder bed fusion also stands out among the reviewed technologies for its improved part accuracy, which is crucial for electrode manufacturing. Since graphite's characteristics vary depending on layer orientation, it should be used only as an admixture and not as a base material in additive manufacturing for more precise fabrication. Controlled ambient temperatures in the LINAC4 extraction system at same time can reduce the risk of thermal stresses that, due to differences in thermal expansion, could lead to structural failures on the material surface.

# References


[1] E. Sargsyan *et al.*, "Linac4 source and low energy experience and challenges," in *Beam Dynamics in Linacs*, Okt 2023, pp. 290–296. [Online]. Available: http://dx.doi.org/10.18429/JACoW-HB2023-WEA4I2

[2] C. Baumgarten, A. Barchetti, H. Einenkel, D. Goetz, and P. Schmelzbach, "A compact electron cyclotron resonance proton source for the paul scherrer institute's proton accelerator facility," *Review of Scientific Instruments*, vol. 82, 2011. [Online]. Available: https://doi.org/10.1063/1.3590777

[3] C. Wiesner *et al.*, "Proton driver linac for the frankfurt neutron source," in *AIP Conference Proceedings*, vol. 1265, Aug 2010, pp. 487–492. [Online]. Available: https://www.researchgate.net/publication/234894129_Proton_Driver_Linac_for_the_Frankfurt_Neutron_Source

[4] Z.M. Zhang *et al.*, "Development of intense proton ecr ion sources at imp," Institute of Modern Physics, Chinese Academy of Sciences, China, Status Report TUPP13, 2012, accessed: 2024-07-22. [Online]. Available: https://accelconf.web.cern.ch/ecris2012/papers/tupp13.pdf

[5] F. Abdelsalam, M. Abdelrahman, and B. Soliman, "An electrostatic lens system for the deceleration of heavy ion beams," *Nuclear Instruments and Methods in Physics*, vol. 8, pp. 199–207, Jan 2014, accessed: 2024-07-22. [Online]. Available: https://www.researchgate.net/publication/263311227_An_electrostatic_lens_system_for_the_deceleration_of_heavy_ion_beams

[6] Z. Bowen, Z. Hong, Z. Pengjiao, L. Wenliang, and A. Sun, "Design and optimization study of a duoplasmatron ion source for high-intensity proton beam," *Nuclear Instruments and Methods in Physics Research Section A: Accelerators, Spectrometers, Detectors and Associated Equipment*, vol. 1010, p. 165550, Sep 2021. [Online]. Available: https://doi.org/10.1016/j.nima.2021.165550

[7] R. Scrivens *et al.*, "Overview of the status and developments on primary ion sources at cern," CERN, Tech. Rep., 2011, accessed: 2024-07-23. [Online]. Available: https://www.researchgate.net/publication/254468833_Overview_of_the_status_and_developments_on_primary_ion_sources_at_CERN

[8] Y. Huang and I. Pokidov, "Extraction electrode system for high current ion implanter," U.S. Patent US7 915 597B2, 2011, Assignee: Axcelis Technologies Inc. [Online]. Available: https://patents.google.com/patent/US7915597B2/en

[9] D. Faircloth, "Ion sources for high-power hadron accelerators," Rutherford Appleton Laboratory, Oxfordshire, UK, Tech. Rep., Feb 2013, accessed: 2024-07-25. [Online]. Available: https://www.researchgate.net/publication/235633927_Ion_sources_for_high-power_hadron_accelerators

[10] F. Junge, M. Auge, and H. Hofsäss, "Sputter hot filament hollow cathode ion source and its application to ultra-low energy ion implantation in 2D materials," *Nuclear Instruments and Methods in Physics Research Section B: Beam Interactions with Materials and Atoms*, vol. 510, pp. 63–68, Jan 2022. [Online]. Available: https://doi.org/10.1016/j.nimb.2021.10.017

[11] Y.J. Kim, D.H. Park, H.S. Jeong, and Y.S. Hwang, "New method of high brightness ion extraction based on bias electrode," *Review of Scientific Instruments*, vol. 77, no. 3, p. 03B507, Mar 2006, accessed: 2024-08-02. [Online]. Available: https://doi.org/10.1063/1.2167387

[12] T. Kenmotsu, N. Miyamoto, and M. Wada, "Erosion of extraction electrodes of ion sources due to sputtering," *AIP Conference Proceedings*, vol. 1321, pp. 325–328, Jan 2011, accessed: 2024-08-01. [Online]. Available: https://doi.org/10.1063/1.3548405

[13] K. Goto, M. Kawai, and K. Tamura, "Ion extraction electrode system and ion implantation device," Japan Patent JP2 001 312 974A, 2001, accessed: 2024-08-01. [Online]. Available: https://patents.google.com/patent/JP2001312974A/en

[14] Stanford Advanced Materials, "Preparation and application of tzm alloy," 2023, accessed: 2024-07-19. [Online]. Available: https://www.samaterials.com/content/preparation-application-of-tzm-alloy.html

[15] Midwest Tungsten Service, "Tungsten (w)," 2024, accessed: 2024-08-05. [Online]. Available: https://www.tungsten.com/material-info/tungsten-w

[16] Plansee Group, "Tungsten: Properties and uses," 2016, accessed: 2024-08-05. [Online]. Available: https://www.plansee.com/en/materials/tungsten.html#content-accordion-2080C930920DC2CEB6089DB50716D062

[17] R. Davey, "What are the mechanical properties of tungsten?" 2023, accessed: 2024-08-05. [Online]. Available: https://www.azom.com/article.aspx?ArticleID=7641

[18] International Molybdenum Association. Role of molybdenum. Accessed: 2024-08-05. [Online]. Available: https://www.imoa.info/molybdenum/molybdenum-properties.php

[19] Royal Society of Chemistry. Molybdenum - element information. Accessed: 2024-08-05. [Online]. Available: https://www.rsc.org/periodic-table/element/42/molybdenum

[20] Wolfram Research, Inc. Technical data for molybdenum. Accessed: 2024-08-05. [Online]. Available: https://periodictable.com/Elements/042/data.html

[21] MatWeb. Molybdenum, Mo; High Purity (UNS R03600). Accessed: 2024-08-05. [Online]. Available: https://www.matweb.com/search/datasheet.aspx?matguid=a6039ca64ad74598aadf05c9e2f6c1a4

[22] Ed Fagan. Molybdenum tzm properties. Accessed: 2024-08-06. [Online]. Available: https://www.edfagan.com/refractory-metal-supplier/molybdenum-tzm/molybdenum-tzm-properties/

[23] A.de Rooij. Molybdenum TZM. Accessed: 2024-08-06. [Online]. Available: https://www.spacematdb.com/spacemat/manudatasheets/Moly_TZM%20364.pdf

[24] Texsa S.R.L. TZM - Titanium- Zirconium-Molybenum Alloy Technical Datasheet. Accessed: 2024-08-06. [Online]. Available: https://texsasrl.it/wp-content/uploads/2018/04/TX_HSM_TZM_it.pdf

[25] F. Carra *et al.*, "Novel materials for collimators at LHC and its upgrades," in *Proceedings of the [Conference: HB2014]*, 2014, accessed: 2024-08-06. [Online]. Available: https://www.researchgate.net/publication/325603988_Novel_materials_for_collimators_at_LHC_and_its_upgrades

[26] F. Carra *et al.*, "Mechanical Engineering and Design of Novel Collimators for HL-LHC," CERN, Tech. Rep. CERN-ACC-2014-0184, 2014, accessed: 2024-08-06. [Online]. Available: https://cds.cern.ch/record/1748367/files/CERN-ACC-2014-0184.pdf

[27] Lenntech. (2024) Titanium - Ti. Accessed: 2024-08-06. [Online]. Available: https://www.lenntech.com/periodic/elements/ti.htm

[28] KYOCERA SGS Precision Tools Europe Ltd. (2024) Titanium properties. Accessed: 2024-08-06. [Online]. Available: https://kyocera-sgstool.co.uk/titanium-resources/titanium-information-everything-you-need-to-know/titanium-properties/

[29] A.M. Helmenstine, "Table of electrical resistivity and conductivity," 2024, accessed: 2024-08-06. [Online]. Available: https://www.thoughtco.com/table-of-electrical-resistivity-conductivity-608499

[30] MatWeb. (2024) Graphite, Carbon, C. Accessed: 2024-08-07. [Online]. Available: https://www.matweb.com/search/DataSheet.aspxMatGUID=3f64b985402445c0a5af911135909344&ckck=1

[31] M.I. Ojovan and A.J.Wickham, "Radiation effects in graphite," International Atomic Energy Agency, 2019, accessed: 2024-08-07. [Online]. Available: https://indico.ictp.it/event/7633/session/1/contribution/17/material/0/0.pdf

[32] E. Solfiti and F. Berto, "Mechanical properties of flexible graphite: review," *Procedia Structural Integrity*, vol. 25, pp. 420–429, 2020. [Online]. Available: https://doi.org/10.1016/j.prostr.2020.04.047

[33] L. Zhao, J. Tang, M. Zhou, and K. Shen, "A review of the coefficient of thermal expansion and thermal conductivity of graphite," *New Carbon Materials*, vol. 37, no. 3, pp. 544–555, Jun 2022. [Online]. Available: https://dx.doi.org/10.1016/S1872-5805(22)60603-6

[34] S. Zhang, N. Ukrainczyk, A. Zaoui, and E. Koenders, "Electrical conductivity of geopolymer-graphite composites: Percolation, mesostructure and analytical modeling," *Construction and Building Materials*, vol. 411, p. 134536, Jan 2024. [Online]. Available: https://doi.org/10.1016/j.conbuildmat.2023.134536

[35] International Atomic Energy Agency (IAEA). (2024) What is graphite. Accessed: 2024-08-07. [Online]. Available: https://nucleus.iaea.org/sites/graphiteknowledgebase/wiki/Guide_to_Graphite/What%20is%20Graphite.aspx

[36] Science Fun, Inc., "Cryogenics with liquid nitrogen," n.d., accessed: 2024-08-12. [Online]. Available: http://members.mrtc.com/anvk/cryogenics/cryogenics.html

[37] F. Emin, "Exploring shrinkage in metals and alloys: Understanding rates and implications," 2023, accessed: 2024-08-12. [Online]. Available: https://www.linkedin.com/pulse/exploring-shrinkage-metals-alloys-understanding-rates-ferdun-emin-mqetf/

[38] Ferguson Performance, "6061 aluminium alloy," accessed: 2024-08-08. [Online]. Available: https://www.fergusonperf.com/the-perforating-process/material-information/specialized-aluminum/6061-aluminium-alloy/

[39] ASM MatWeb, "Aluminum 6061-T6," accessed: 2024-08-07. [Online]. Available: https://asm.matweb.com/search/SpecificMaterial.asp?bassnum=ma6061t6

[40] Gabrian International, "6061 Aluminum: Get to Know its Properties and Uses," accessed: 2024-08-07. [Online]. Available: https://www.gabrian.com/6061-aluminum-properties/

[41] NDT Supply, "Conductivity and resistivity values for aluminum and alloys," 2002, accessed: 2024-08-07. [Online]. Available: https://content.ndtsupply.com/media/Conductivity_Al%20Reference%20Chart.pdf

[42] K. Narender, A. Rao, K. Rao, and N. Krishna, "Temperature dependence of density and thermal expansion of wrought aluminum alloys 7041, 7075 and 7095 by gamma ray attenuation method," *Journal of Modern Physics*, vol. 4, no. 3, pp. 331–336, 2013, accessed: 2024-08-07. [Online]. Available: http://dx.doi.org/10.4236/jmp.2013.43045

[43] Giesserei Hegi AG, "Technisches merkblatt," n.d., accessed: 2024-08-07. [Online]. Available: https://hegi.ch/media/1199/technisches-merkblatt-alsi7mg.pdf

[44] MakeItFrom, "EN AC-42000 (AISi7Mg) Cast Aluminum," 2020, accessed: 2024-08-07. [Online]. Available: https://www.makeitfrom.com/material-properties/EN-AC-42000-AISi7Mg-Cast-Aluminum

[45] Sunrise Metal, "Aluminum Alloy AlSi12," 2024, accessed: 2024-08-07. [Online]. Available: https://www.sunrise-metal.com/aluminum-alloy-alsi12

[46] K. Naoum and G. Paulsen, "Copper: Definition, composition, types, properties, and applications," 2024, accessed: 2024-08-06. [Online]. Available: https://www.xometry.com/resources/materials/what-is-copper/

[47] J. Levine, "Copper's coefficient of thermal expansion varies, but to little effect," 2022, accessed: 2024-08-06. [Online]. Available: https://www.wje.com/assets/pdfs/articles/WJE-PRIMER-Coppers-Coefficient-of-Thermal-Varies.pdf

[48] Copper Association eV. (2023) Copper - Properties. Accessed: 2024-08-06. [Online]. Available: https://kupfer.de/kupferwerkstoffe/kupfer/eigenschaften/?lang=ne

[49] MatWeb. (2024) Copper, cu; annealed. Accessed: 2024-08-06. [Online]. Available: https://www.matweb.com/search/datasheet_print.aspx?matguid=9aebe83845c04c1db5126fada6f76f7e

[50] K.T. Slattery, D.E. Driemeyer, and J.W. Davis, "Process of bonding copper and tungsten," U.S. Patent US6 089 444A, Jul, 2000, Assignee: McDonnell Douglas Corporation, St.Louis, Mo. [Online]. Available: https://patents.google.com/patent/US6089444A/en

[51] L. Guirong *et al.*, "Tungsten-aluminum alloy and preparation method for same," People's Republic of China Patent CN103 773 983A, May, 2014, Assignee: Advanced Technology and Materials Co. Ltd. [Online]. Available: https://patents.google.com/patent/CN103773983A/en

[52] E. Koetter, D. Drakova, and G. Doyen, "Theory of atom transfer between an aluminum and a tungsten electrode," *Surface Science*, vol. 331-333, pp. 679–684, 1995. [Online]. Available: https://doi.org/10.1016/0039-6028(95)00163-8.

[53] Midwest Tungsten Service, "Fabricating tungsten alloys," 2022, accessed: 2024-08-12. [Online]. Available: https://www.tungsten.com/blog/fabricating-tungsten-alloy

[54] General Carbide Corporation, "A Designer's Guide to Tungsten Carbide," 2019, accessed: 2024-08-12. [Online]. Available: https://www.generalcarbide.com/wp-content/uploads/2019/04/GeneralCarbide-Designers_Guide_TungstenCarbide.pdf

[55] J.A. Shields Jr., "Applications of molybdenum metal and its alloys," International Molybdenum Association, Tech. Rep., 2013, accessed: 2024-08-12. ISBN: 978-1-907470-30-1. [Online]. Available: https://www.imoa.info/download_files/molybdenum/Applications_Mo_Metal.pdf

[56] Ceramaterials, "Technical Data Sheet: Molybdenum, TZM and Mola," Ceramaterials, Tech. Rep., 2021, accessed: 2024-08-12. [Online]. Available: https://www.ceramaterials.com/wp-content/uploads/2021/12/CM_TDS_Molybdenum_TZM__Mola_12_21.pdf

[57] P. Brett and K. Jan and S. Luffrum, "Why shrink-fit steel flanges to titanium pipe?" Jul 2015, accessed: 2024-08-12. [Online]. Available: https://www.slideshare.net/slideshow/dot-international-2010-titanium-shrinkfit/50458603

[58] S. Carbon, "Sigrafine-the motion facilitators," Graphite Materials and Systems, Tech. Rep., 2018, accessed: 2024-08-12. [Online]. Available: https://www.sglcarbon.com/data/pdf/SGL-Brochure-SIGRAFINE-The-Motion-Facilitators-EN.pdf

[59] J.H. Fichet (CERN), "Last shrink fitting operation of the run 3 lhc beam dump spares," 2023, accessed: 2024-08-12. [Online]. Available: https://cds.cern.ch/record/2851549

[60] I. Meyer *et al.*, "Additive manufacturing of multi-material parts – design guidelines for manufacturing of 316l/cucrzr in laser powder bed fusion," *Heliyon*, vol. 9, no. 8, p. e18301, 2023, accessed: 2024-08-14. [Online]. Available: https://doi.org/10.1016/j.heliyon.2023.e18301

[61] A. Nazir *et al.*, "Multi-material additive manufacturing: A systematic review of design, properties, applications, challenges, and 3d printing of materials and cellular metamaterials," *Materials & Design*, vol. 226, p. 111661, 2023. [Online]. Available: https://doi.org/10.1016/j.matdes.2023.111661

[62] N.D. Dejene and H.G. Lemu, "Current status and challenges of powder bed fusion-based metal additive manufacturing: Literature review," *Metals*, vol. 13, no. 2, 2023. [Online]. Available: https://doi.org/10.3390/met13020424

[63] P. Gradl, A. Cervone, and P. Colonna, "Influence of build angles on thin-wall geometry and surface texture in laser powder directed energy deposition," *Materials & Design*, vol. 234, p. 112352, 2023. [Online]. Available: https://doi.org/10.1016/j.matdes.2023.112352

[64] A. Nassar and E. Reutzel, "Beyond layer-by-layer additive manufacturing – voxel-wise directed energy deposition," in *International Solid Freeform Fabrication Symposium*, 2015, pp. 273–283, accessed: 2024-08-14. [Online]. Available: https://utw10945.utweb.utexas.edu/sites/default/files/2015/2015-22-Nassar.pdf

[65] K. Sanjeeviprakash, A. Kannan, and N. Shanmugam, "Additive manufacturing of metal-based functionally graded materials: overview, recent advancements and challenges," *Journal of the Brazilian Society of Mechanical Sciences and Engineering*, vol. 45, p. 241, Apr 2023. [Online]. Available: https://doi.org/10.1007/s40430-023-04174-1

[66] R. Anderson *et al.*, "Characteristics of bi-metallic interfaces formed during direct energy deposition additive manufacturing processing," *Metallurgical and Materials Transactions B*, vol. 50, p. 1921–1930, May 2019. [Online]. Available: https://doi.org/10.1007/s11663-019-01612-1